Available online at www.sciencedirect.com

SciVerse ScienceDirect

Ceramics International 39 (2013) 4457–4464

CERAMICS INTERNATIONAL

www.elsevier.com/locate/ceramint

Effect of sintering temperature on the mechanical and physical properties of WC–10%Co through micro-powder injection molding (μPIM)

Shye Yunn Heng, Norhamidi Muhamad, Abu Bakar Sulong*, Abdolali Fayyaz, SriYulis. M. Amin

Department of Mechanical and Materials Engineering, Faculty of Engineering and Built Environment, Universiti Kebangsaan Malaysia, 43600 Bangi, Selangor, Malaysia

Received 28 September 2012; received in revised form 12 November 2012; accepted 12 November 2012
Available online 29 November 2012

Abstract

Micro-powder injection molding (μPIM) is a net shape process that is able to mass produce the micro-components of metals, ceramics, and carbides, with intrinsic and complex shapes at lower cost compared with machining, casting and powder compaction. However, the μPIM of hardmetals, such as WC–Co is more challenging due to their high thermal conductivity and ease of agglomeration. Thus, WC–Co alloy mixed with wax-based binder feedstock was selected. The formed feedstock exhibited pseudoplastic flow and was successfully injection-molded (green part). Wax-based binder was able to retain the structure of the green part during solvent and thermal debinding without any shrinkage and collapse of structure. It was sintered at 1380 °C, 1400 °C and 1420 °C. The shrinkage of the sintered part was approximately 25–31% compared with the brown part. In the microstructure analysis of the sintered part
at 1380 °C, micro-pooling of Co and porosity were observed. An increase in the sintering temperature accelerated the melted Co distribution between the grain boundary of WC, thus increasing the eta (η) phases and the grain growth. The sintered part of WC–10%Co shrank by 25–31%. The overall mechanical properties of the sintered part increased with increasing sintering temperature. The sintered parts exhibited an average transverse rupture strength (TRS) of 2042 MPa. The average hardness measured was 1667 HV, which is higher than 1620 HV (theoretical hardness of the WC alloy). The average densification achieved was approximately 96% (13.85 g cm^{-3}) of the theoretical density.
© 2012 Elsevier Ltd and Techna Group S.r.l. All rights reserved.

Keywords: A. Sintering; B. Microstructure; Micro-powder injection molding (μPIM); Tungsten carbide

1. Introduction

The development of microsystem technology (MST) requires components with sizes or features in the micrometer range. The application of machining and casting in MST is hindered by excessive waste material, time constraints, high production costs and geometry limitations. Therefore, μPIM is a promising net shape process, that is able to meet the requirements of MST [1]. The technology and knowledge behind μPIM involve a combination of powder metallurgy and micro-plastic injection molding. Micro-sized structures can be replicated through this process. The process can greatly enhance the capabilities and properties of the micro-components by mass-producing metal, ceramic, and carbide components with complex shapes [2]. In general, μPIM consists of four stages: mixing of powder and binder to prepare the feedstock, injection molding to replicate the mold inserts, debinding to remove the binder constituents and sintering to promote the diffusion of powder to achieve the required properties [3,4]. Tungsten carbide (WC) is known as "hardmetal", which is expensive and extremely difficult to machine due to its high hardness. Thus, most WC is produced through powder metallurgy (PM) processes, such as powder compaction. However, the complexity of the WC product is limited by the process ability of PM [5,6]. Currently, a

*Corresponding author. Tel.: +603 89216678; fax: +603 89259659.
E-mail address: abubakar@eng.ukm.my (A.B. Sulong).

0272-8842/$ - see front matter © 2012 Elsevier Ltd and Techna Group S.r.l. All rights reserved.
http://dx.doi.org/10.1016/j.ceramint.2012.11.039

growing demand exists for finely grown WC–Co powders in related areas: miniature drills, wear-resistant parts and coatings, rock drill, tool for cutting cast iron, and so on [7]. Thus, the two objectives of this study are to investigate the debinding behavior during the removal of binder and the effect of the sintering temperature on the mechanical and physical properties of the sintered part.

2. Experimental procedure

WC (99.5% metal basis, < 1 μm, irregular particle with an angular shape) and Co (99.8% metal basis, 1.6 μm, irregular rounded shape) purchased from Alfa Aesar were used. WC and Co were subjected to pre-alloying to form WC–10%Co through the mechanical blending method. Blending was applied to ensure a uniform distribution of WC and Co in the end product [7]. The morphology of the powders was observed using a Zeiss Supra 55-VP Field-Emission Scanning Electron Microscope (FESEM). The pycnometer density of the WC–10%Co powder was 12.47 g/cm^3, measured using Micrometrics AccuPyc1330 He-Pycnometer, purged under helium gas. Pycnometer density obtained is lower than theoretical density of powder (14.45 g/cm^3) due to gas absorbed on the surface of powder [8]. The apparent and tap densities were 2.42 and 3.24 g/cm^3 respectively. The WC–10%Co powder is a high-density mixed powder; thus, a wax-based binder was chosen. The loose WC–10%Co powder was mixed with paraffin wax (PW), polyethylene (PE), oleic acid, and stearic acid (SA) to form the feedstock, which was later used for injection molding. The WC–10%Co feedstock was injected into a micro dumb bell shape that was 9 mm long, 2.82 mm diameter and 0.8 mm thick at the micro-injection molding DSM Explore [9]. The injection molding parameters used were: pressure (8, 9, and 10 bar), melt temperature (140, 145, and 150 °C), mold temperature (110, 113, and 116 °C), and packing time (7 s). The binder was removed in the solvent (heptane) at 80 °C for 20 min, followed by thermal debinding as shown in Fig. 1. The brown part was sintered at 1380–1420 °C at heating rate of 10 °C/min and holding time of 2 min. The surface microstructure of WC–10%Co was observed after grinding, polishing and etching with Murakami reagent. The TRS of the micro-component was determined using Instron 5567 at a speed rate of 1 mm/min with a 1 kN load cell. The hardness of the micro-component was determined using a MITAKA Vickers Tester with a 3 kgf dwell load and 15 s dwell time. The surface roughness was examined using a Mitutoyo SV-C3100 surface profiler at travel velocity of 1 mm/s and travel distance of 5 mm.

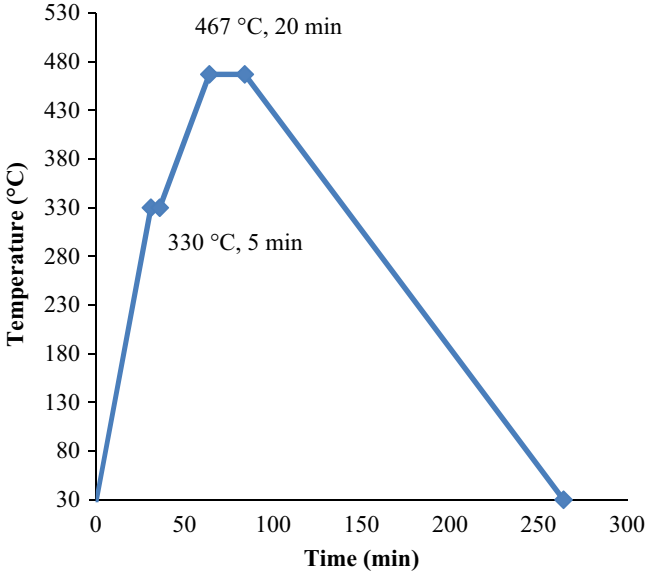

Fig. 1. Thermal debinding cycle for WC–10%Co.

3. Results and discussion

3.1. Changes in the microstructure of WC–10%Co

Our previous work showed that the feedstock formed has a pseudoplastic flow behavior with a flow index of nearly 0.5 [10]. Pseudoplastic was the desired flow to ensure the mixture flow during injection molding, especially for the micro-mold, because the area of the entry mold was small [11]. A high mold temperature in the range of 110–116 °C was used to produce the green part, as shown in Fig. 2(a) due to the high thermal conductivity of WC–10%Co, which is 103 Wm^{-1} K^{-1} [12]. The high thermal conductivity of WC–10%Co can speed up the heat transfer during injection. The mold temperature needs to be increased to compensate for the heat loss during the

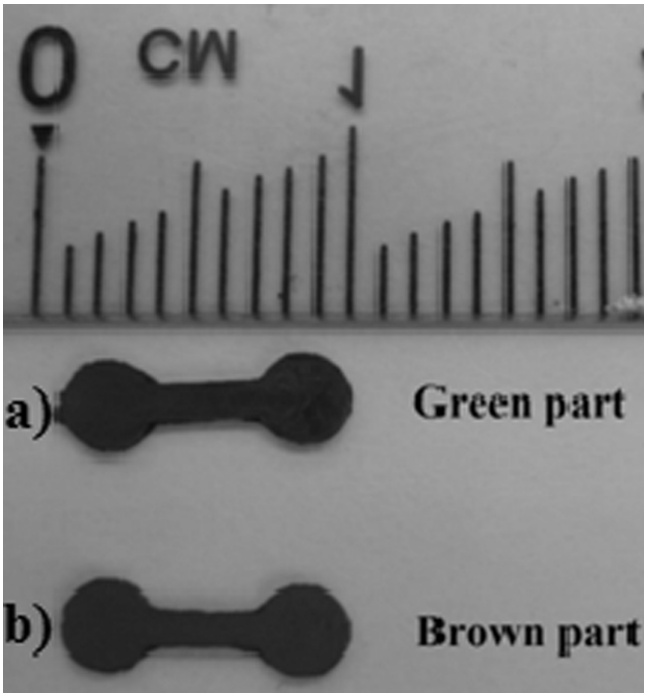

Fig. 2. Geometry comparison between: (a) the green part (after injection molding) and (b) the brown part (after thermal debinding).

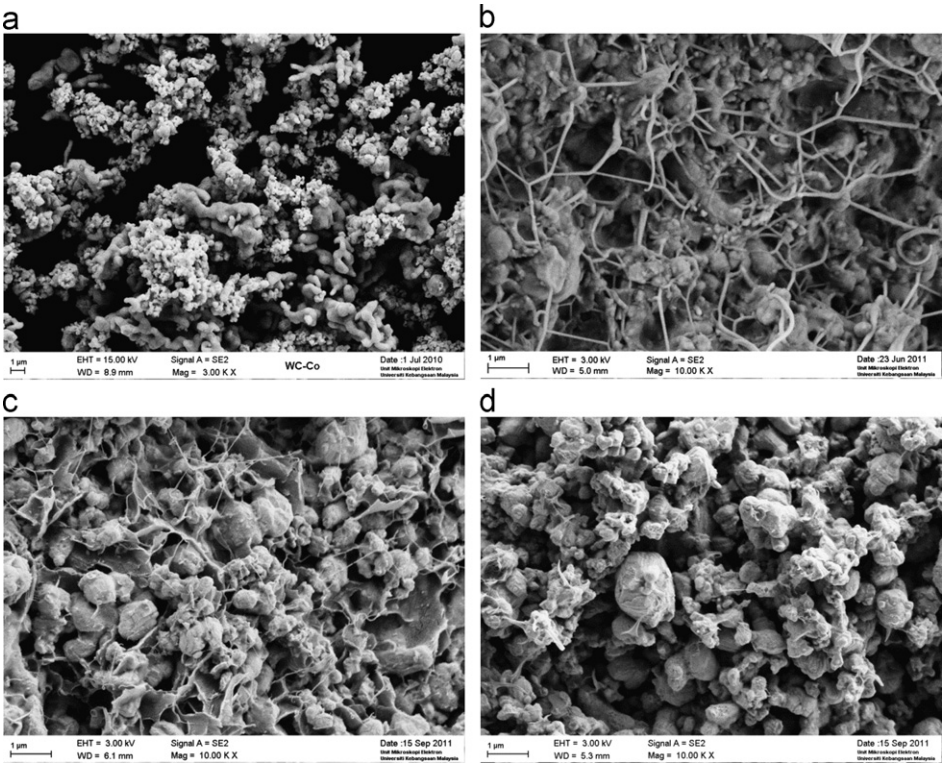

Fig. 3. SEM image of: (a) WC–10%Co loose powder; (b) the green part; (c) the brown part (after solvent debinding) and (d) the brown part (after thermal debinding).

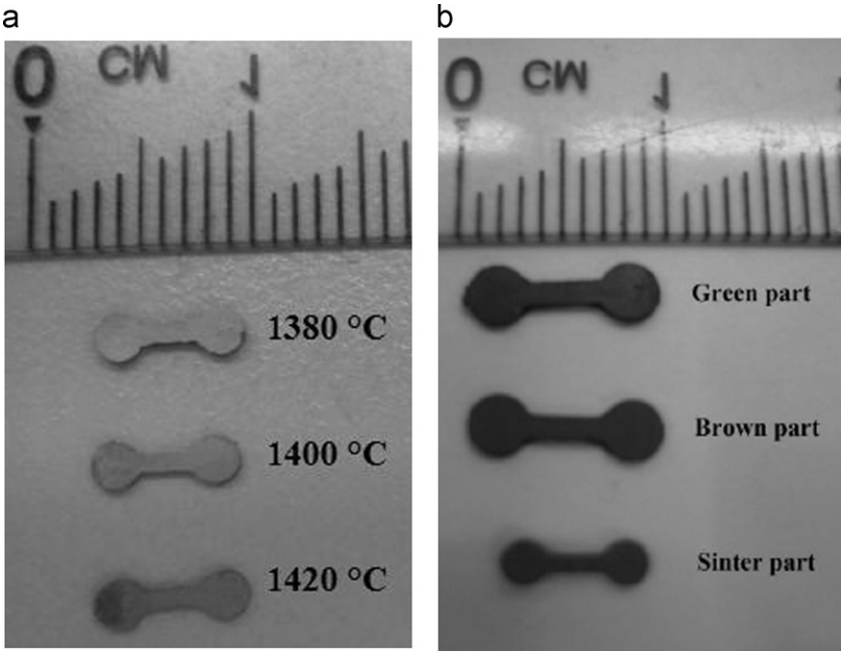

Fig. 4. (a) Sintered part of WC–10%Co after sintering at 1380, 1400, and 1420 °C and (b) representative physical changes of the green, brown and sintered parts.

micro-injection molding [13]. No geometry change was observed in the green and brown parts, as shown in Fig. 2.

The debinding behavior in the green part during solvent and thermal debinding are shown in Fig. 3. The loose powder of WC–10%Co was in an agglomerated state, as shown in Fig. 3(a). The presence of moisture was the main cause for the agglomeration, and this became significant for the fine powder because fine powder has a high surface area [14].

Fig. 3(b) shows the compounded feedstock after injection molding. The particles of WC were covered by PW and the remaining PE binders held the powder in a "net" form. A low contact angle between PW and WC could be seen using the wetting method, which allows more powder to fill-in, and high powder loading was achieved with a low contact angle of the binder [15]. The low contact angle explains why high powder loading can be achieved with a wax-based binder system, compared with a water-based binder [6]. The mechanical strength of PE served as the backbone of the green part to provide structural strength and handlling support during the thermal debinding and the sintering process. Fig. 3(b) shows that the inter-distance of the particles was increased after injection pressure was applied. After solvent debinding, the soluble binder was diffused out from the part. The PW layer was lost. The brown part of the leaf with the "net" and the powder is shown in Fig. 3(c). Thermal debinding was applied to decompose the primary binder PE. Finally, only WC–Co powder particles were observed in Fig. 3(d) after thermal debinding.

3.2. Sintering of WC–10%Co

Fig. 4(a) shows the sintered part of the WC–10%Co after liquid phase sintering at different sintering temperatures. During liquid phase sintering, melted Co flows to fill the pores in the brown part. A rearrangement of WC occurs through liquid formation to achieve the final densification [16]. Fig. 4(b) clearly shows that the sintered part shrunk and became dense after sintering. Melted Co was identified between the grains of the particle WC of the sintered part using the mapping method associate with FESEM as shown in Fig. 5. Clearly, the melted Co was located between the grain boundaries of WC. Co functions as the binder in WC–Co and ensures sufficient toughness in WC–Co [17–20]. The measured shrinkage of the sintered part was approximately 25–31%. High shrinkage occurred due to the low powder loading (44 vol%) in this study. A shrinkage range of 15–25% is common in the production of micro-miniature parts using μPIM [21,22]. Swelling and defects were observed in the sintered WC–10%Co part, as shown in Fig. 6. Swelling occurred due to the high solubility of Co in WC particles and the capillary force exerted by the liquid on the solid WC. Defects occurred on the sintered part due to the inhomogeneity of the distribution between the binder polymer and the powder. They may also have been caused by entrapped gas after the binder was removed.

3.3. Microstructure of sintered WC–10%Co

Fig. 7 shows the microstructure of the sintered part at different sintering temperatures after etching with the

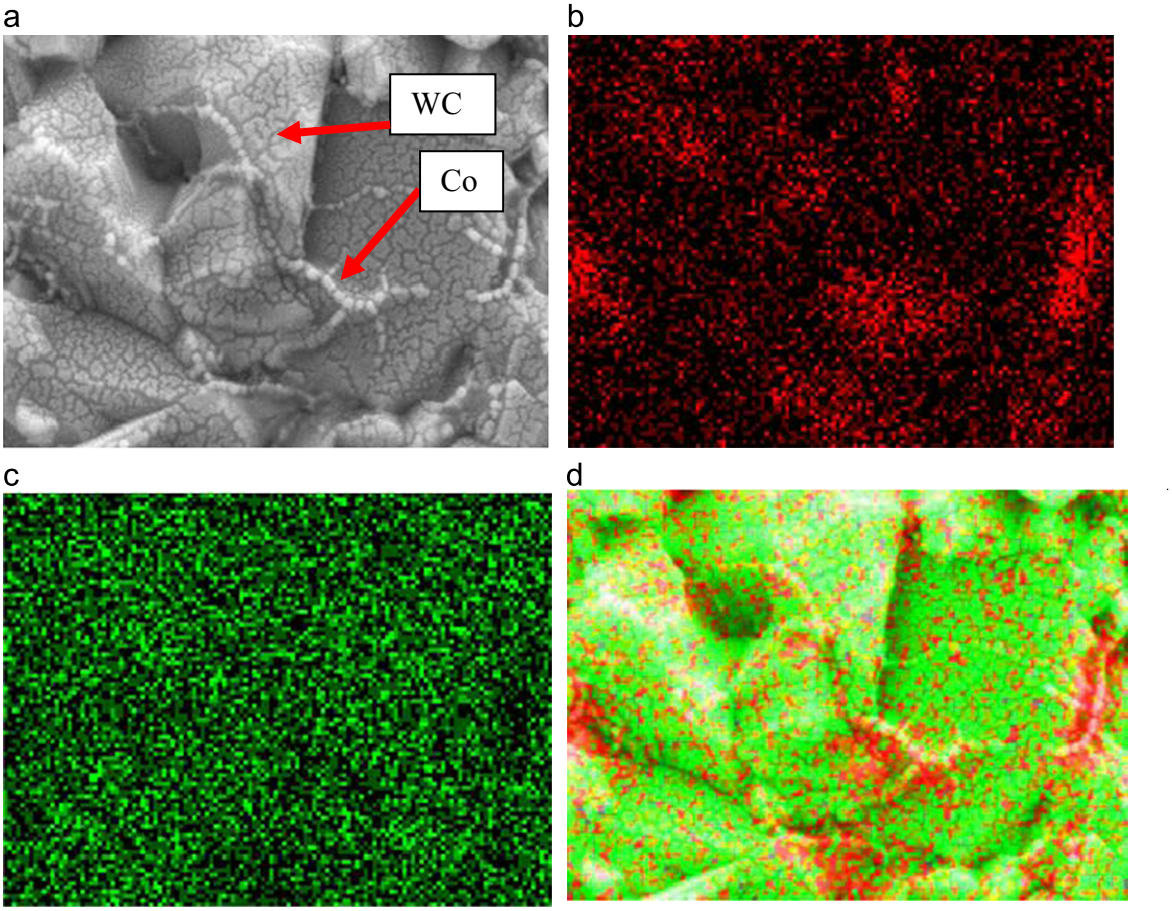

Fig. 5. Distribution of WC and Co through the mapping method associated with FESEM.

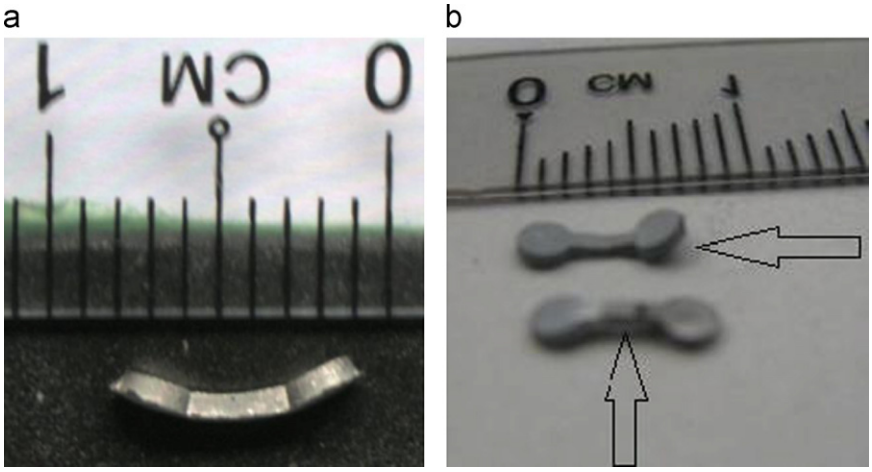

Fig. 6. (a) Swelling of the part after liquid sintering at 1350 °C for 5 min, and (b) defects of the part after sintering at 1380 °C.

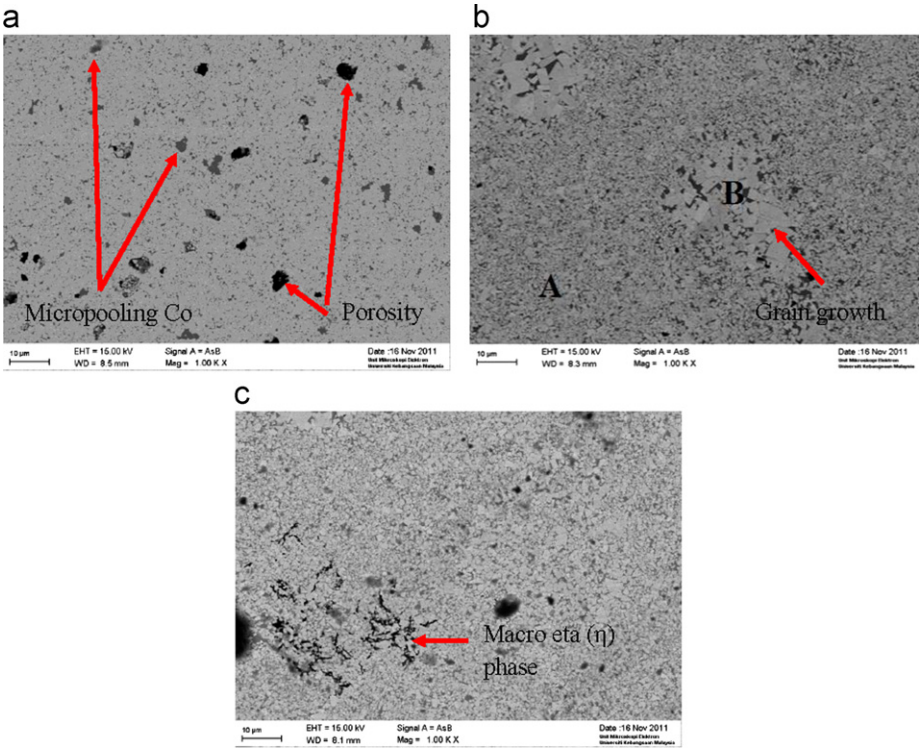

Fig. 7. Microstructure of WC–10%Co at (a) 1380, (b) 1400, and (c) 1420 °C sintering temperatures.

Murakami reagent. According to the results in Fig. 7, porosity was found at a lower temperature (Fig. 7(a)), whereas grain growth and eta (η) phase were found at a higher temperature than the sintering temperature used (Fig. 7(b) and (c)). The pore size decreased with increasing sintering temperature because melted Co covers the pores evenly because of the high temperature. The porosity was reduced with increasing homogeneity of Co [23]. The capillary force of Co acted on the solid WC to eliminate porosity [16]. The porosity found on the part sintered at 1380 °C (Fig. 7(a)) may have been caused by the micropooling of Co in this study, in which the agglomerated Co was not well distributed. Co is a metal that tends to absorb moisture and to agglomerate easily [24]. Grain growth occurred at high sintering temperatures of, 1400 °C and 1420 °C. The sizes of the normal grains were 545.2, 849.3 and 957.5 nm, which grew to 2.357, 3.448 and 5.394 μm, respectively, as shown in Fig. 8. Grain growth was observed at a certain location in the microstructure of the sintered part, which may be due to the agglomeration of powder at in said region that tends to generate grain growth. Agglomerated powder will reduce the interfacial energy (area) at the solid–liquid interface, which is the driving force for grain growth [25]. The difference in size

boundary curvature increase will help coalescence [16]. The clustering of the grain will enhance the coalescence among particles and will contribute to the grain growth [26,27]. This occurrence is significant for WC, which has a size of less than 1 μm and abroad particle size range. A high sintering temperature can fasten the growth process, which explains why grain growth occurred at a high sintering temperature. Moreover, the macro η phase was found in the part sintered at 1420 °C, as shown in Fig. 9.The η phase is also known as porosity and is a form of compound ternary. The η phase formed resulted from the decarburizing process, whereby the oxygen absorbed on powder combines with carbon to form carbon monoxide and carbon dioxide during the sintering process. Excessive carbon loss will result from the formation of the η phase [28].

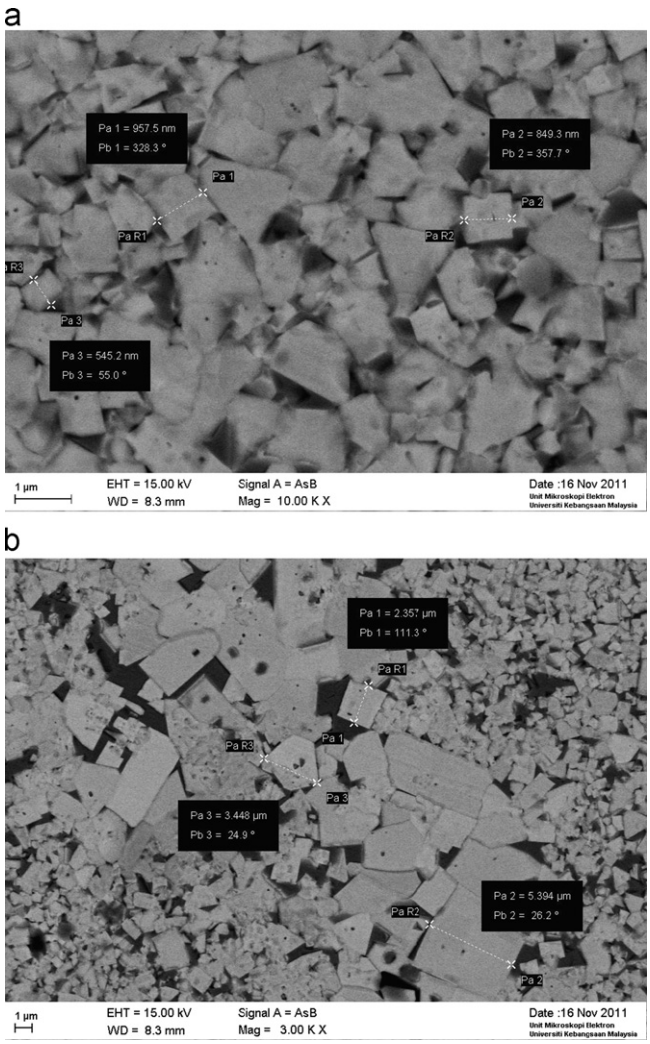

Fig. 8. Enlargement of the grain size of WC–10%Co at 1400 °C sintering temperature: (a) the sizes of the normal grains (point A) were 545.2, 849.3, 957.5 nm and (b) the sizes of grain growth (point B) were 2.357, 3.448 and5.394 μm.

3.4. Mechanical property of WC–10%Co

The resultant mechanical properties of the sintered part of WC–10%Co at different sintering temperatures are summarized in Table 1. The density increased with increasing sintering temperature because large quantities of Co melted at high temperature and flowed to fill the pores [29]. The hardness value obtained was near the theoretical value of HV_{30} of 1620 ± 50 kg/mm^2, according to the *Ultra Carbide Inc*, ISO 3878. However, the hardness of the sintered part decreased at 1420 °C, which may be due to the grain growth, as coarse grain is inferior in hardness to fine grain [30,31]. The TRS gradually increased with increasing sintering temperature. However, the overall value of TRS (2000 MPa on average) was relatively lower than the theoretical value of the cast part. The TRS strength for WC–10%Co (grain size = 0.5–0.8 μm) has been reported to be approximately 3500 MPa [32].The main reason why the TRS value was lower than the theoretical value is the loss of Co to the graphite stage during the sintering process. Sachet et al. [33] reported that the spread of Co and the formation of the Co layer can occur within 30–120 s. A high rate of cooling at approximately 25–50 °C/min was

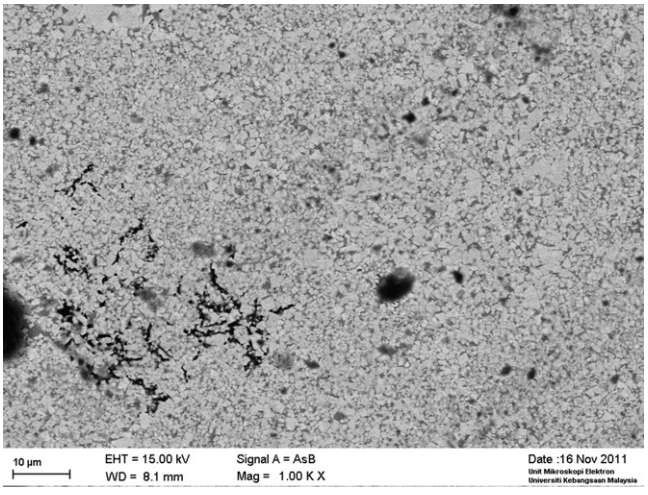

Fig. 9. The macro eta phase occured at 1420 °C sintering temperature.

Table 1
Mechanical properties of the sintered WC–10%Co.

Sintering temperature (°C)	Density (g/cm^3)	Densification (%)	Surface roughness, Ra (μm)	Hardness, HV	Tranverse rupture strength (MPa)
1380	13.78 ± 0.15	95	1.69 ± 0.48	1655.2 ± 73.5	1947.0 ± 487.0
1400	13.88 ± 0.15	96	1.29 ± 0.21	1743.3 ± 93.2	2089.4 ± 487.9
1420	13.89 ± 0.17	96	1.17 ± 0.18	1604.7 ± 61.2	2090.9 ± 368.8

needed to avoid the spread of Co [34]. Significant loss in Co severely affected the TRS. A composition of Co is required to alter the property of WC–Co to withstand the toughness. The mechanical strength achieved in this study was similar to WC–5%Co. In addition, the presence of porosity, micro-pooling of Co, and eta phase also affected the strength performance [35]. Table 1 also shows that the surface roughness of the sintered part decreased with increasing sintering temperature, because the localized melted Co had covered the surface. All the sintered parts achieved a surface roughness of > 1 μm. Theoretically, the roughness of the cast part should be less than 1 μm, because WC with an average particle size < 1 μm was used. This phenomenon may have been due to the low powder loading (44%, in this study), which caused the porosity to appear on the surface, allowing grain growth to occur [36].

4. Conclusion

The debinding behavior of PW and PE binders was observed using SEM. No physical changes were observed after the solvent and thermal debinding processes. Thus, the binder system used in this study was able to function as a structural mechanical medium prior to sintering. The effect of different sintering temperatures on microstructure and mechanical property were studied in detail. The grain growth (in terms of grain size) during the diffusion of WC increased with increasing sintering temperature. The overall mechanical properties improved with increasing sintering temperature. However, the low powder loading (44%) in this study, compared with the theoretical value, caused low TRS and surface roughness. Further studies on finding appropriate methods that will increase powder loading must be conducted because powder loading in μPIM greatly affects the mechanical and physical properties of the sintered part.

Acknowledgments

The authors would like to express their gratitude for the UKM-AP-NBT-11–2009 and FRGS/1/2011/TK/UKM/01/6 Grants from the Malaysian Ministry of Higher Education (MOHE).

References

[1] Q. Wang, H.Q. Yin, X.H. Qu, J.L. Johnson, Effects of mold dimensions on rheological of feedstock in micro powder injection molding, Powder Technology 193 (2009) 15–19.
[2] R. Zauner, Micro powder injection moulding, Microelectronic Engineering 83 (2006) 1442–1444.
[3] Z.Y. Liu, N.H. Loh, S.B. Tor, K.A. Khor, Y. Murakoshi, R. Maeda, T. Shimizu, Micro-powder injection molding, Journal of Materials Processing Technology 127 (2002) 165–168.
[4] H. Abolhasani, N. Muhamad, A new starch-based binder for metal injection molding, Journal of Materials Processing Technology 210 (2010) 961–968.
[5] X. Qu, J. Gao, M. Qin, C. Lei, Rheological behavior and PIM processing of WC–TiC–Co powder feedstock, Journal of University of Science and Technology Beijing 11 (2004) 334–337.
[6] M. Youseffi, I.A. Menzies, Injection molding of WC–6Co powder using two new binder systems based on montanester waxes and water soluble gelling polymers, Powder Metallurgy 40 (1997) 62–65.
[7] C. Kung, T.T. Liao, K.H. Tseng, K.Y. Chen, M.S. Chuang, The Influences of powder mixing process on the quality of W–Cu composites, Transactions of the Canadian Society for Mechanical Engineering 33 (2009) 361–375.
[8] M.J. Yang, R.M. German, Nanophase and superfine cemented carbides processed by powder injection molding, International Journal of Refractory Metals and Hard Materials 16 (1998) 107–117.
[9] M.H.I. Ibrahim, N. Muhamad, A.B. Sulong, K.R. Jamaludin, N.H.M. Nor, S. Ahmad, M.R. Harun, H. Zakaria, Parameter optimization towards highest micro MIM density by using Taguchi method, Key Engineering Materials 443 (2010) 705–710.
[10] S.Y. Heng, N. Muhamad, A.B. Sulong, A. Fayyaz, P.L. Haw, Critical solid loading and rheological study of WC–10%Co, Applied Mechanics and Materials 52–54 (2011) 97–102.
[11] R.M. Gresham, Learning more about viscosity, Tribology & Lubrication Technology 61 (2005) 24–27.
[12] J.F. Shackelford, W. Alexander, Materials Science and Engineering Handbook, CRC Press, New York, 2001.
[13] A. Rota, T.V. Duong, T. Hartwig, Micro powder metallurgy for the replicative production of metallic microstructures, Microsystem Technologies 8 (2002) 323–325.
[14] P.S. Jupiter, V.A. Sundar, K.S. Pavan, A.T. Julian, R.M. German. Understanding homogeneity of powder–polymer mixtures-effect of mixing on tungsten powder injection molding feedstock, Congresso Anual da ABM, Internacional São Paulo, Julho, 2002.
[15] B. Zhu, X. Qu, Y. Tao, Powder injection molding of WC–8%Co tungsten cemented carbide, International Journal of Refractory Metals and Hard Materials 20 (2002) 389–394.
[16] R.M. German, Sintering Theory and Practice, John Wiley & Sons, Pennsylvania, 1996.
[17] A. Upadhyaya, D. Sarathy, G. Wagner, Advances in alloy design aspects of cemented carbides, Materials & Design 22 (2001) 511–517.
[18] N. Chuankrerkkul, P.F. Messer, H.A. Davies, Application of polyethylene glycol and polymethyl methacrylate as binder for powder injection molding of hardmetals, Chiang Mai Journal of Science 35 (2008) 188–195.
[19] N. Chuankrerkkul, P.F. Messer, H.A. Davies, Flow and void formation in powder injection moulding feedstocks made with PEG/PMMA binder Part 2—slip band model, Powder Metallurgy 51 (2008) 72–77.
[20] T. Li, Q. Li, J.Y.H. Fuh, P.C. Yu, L. Lu, Two-material powder injection molding of functionally graded WC–Co components, International Journal of Refractory Metals and Hard Materials 27 (2009) 95–100.
[21] V. Piotter, T. Gietzelt, L. Merz, Micro powder injection moulding of metals and ceramics, Sadhana 28 (2003) 299–306.
[22] R. Heldele, M. Schulz, D. Kauzlaric, J.G. Korvink, J. Haußelt, Micro powder injection molding: process characterization and modeling, Microsystem Technologies 12 (2006) 941–946.
[23] D.F. Carroll, Sintering and microstructural development in WC/Co-based alloys made with superfine WC powder, International Journal of Refractory Metals and Hard Materials 17 (1999) 123–132.
[24] A.G.P. da Silva, W.D. Schubert, B. Lux, The role of the binder phase in the WC–Co sintering, Materials Research 4 (2001) 59–62.
[25] R. Bollina, R.M. German, Heating rate effects on microstructural properties of liquid phase sintered tungsten heavy alloys, International Journal of Refractory Metals and Hard Materials 22 (2004) 117–127.
[26] J.L. Johnson, L.G. Campbell, S.J. Park, R.M. German, Grain growth in dilute tungsten heavy alloys during liquid-phase sintering under microgravity conditions, Metallurgical and Materials Transactions A 40A (2009) 426–437.

[27] X. Wang, Z.Z. Fang, H.Y. Sohn, Grain growth during the early stage of sintering of nanosized WC–Co powder, International Journal of Refractory Metals & Hard Materials 26 (2008) 232–241.
[28] J.L. Fan, B.Y. Huang, H.C. Cheng, T. Liu, Debinding process and carbon content control of hardmetal components by powder injection molding, Powder Injection Moulding International 1 (2007) 57–62.
[29] M. Mahmoodan, H. Aliakbarzadeh, R. Gholamipour, Sintering of WC–10%Co nano powders containing TaC and VC grain growth inhibitors, Transactions of Nonferrous Metals Society of China 21 (2011) 1080–1084.
[30] X.L. Shi, G.Q. Shao, X.L. Duan, Z. Xiong, H. Yang, Characterizations of WC–10Co nanocomposite powders and subsequently sinter-hip sintered cemented carbide, Materials Characterization 57 (2006) 358–370.
[31] A. Petersson, J. Ågren, Modelling WC–Co sintering shrinkage—effect of carbide grain size and cobalt content, Materials Science and Engineering A 452–453 (2007) 37–45.
[32] G. Gille, B. Szesny, K. Dreyer, H. van den Berg, J. Schmidt, T. Gestrich, G. Leitner, Submicron and ultrafine grained hardmetals for microdrills and metal cutting inserts, International Journal of Refractory Metals and Hard Materials 20 (2002) 3–22.
[33] E. Sachet, W.D. Schubert, G. Mühlbauer, J. Yukimura, Y. Kubo, On the formation and in situ observation of thin surface layers of cobalt on sintered cemented carbides, International Journal of Refractory Metals and Hard Materials 31 (2012) 96–108.
[34] D.S. Janisch, W. Lengauer, K. Rödiger, K. Dreyer, H. van den Berg, Cobalt capping: why is sintered hardmetal sometimes covered with binder, International Journal of Refractory Metals & Hard Materials 28 (2010) 466–471.
[35] Z.Z. Fang, Correlation of transverse rupture strength of WC–Co with hardness, International Journal of Refractory Metals & Hard Materials 23 (2005) 119–127.
[36] A. Rota, T.V. Duong, T. Hartwig, Wear resistant tools for reproduction technologies produced by micro powder metallurgy, Microsystem Technologies 7 (2002) 225–228.